

UC Irvine

UC Irvine Previously Published Works

Title

Multimodal CARS microscopy determination of the impact of diet on macrophage infiltration and lipid accumulation on plaque formation in ApoE-deficient mice[S]

Permalink

<https://escholarship.org/uc/item/7bb9b8kv>

Journal

Journal of Lipid Research, 51(7)

ISSN

0022-2275

Authors

Lim, Ryan S
Kratzer, Adelheid
Barry, Nicholas P
et al.

Publication Date

2010-07-01

DOI

10.1194/jlr.m003616

Copyright Information

This work is made available under the terms of a Creative Commons Attribution License, available at <https://creativecommons.org/licenses/by/4.0/>

Peer reviewed

Multimodal CARS microscopy determination of the impact of diet on macrophage infiltration and lipid accumulation on plaque formation in ApoE-deficient mice[§]

Ryan S. Lim,^{*,†} Adelheid Kratzer,[§] Nicholas P. Barry,[§] Shinobu Miyazaki-Anzai,[§] Makoto Miyazaki,[§] William W. Mantulin,^{*} Moshe Levi,[§] Eric O. Potma,^{*,**} and Bruce J. Tromberg^{1,*,††}

Laser Microbeam and Medical Program (LAMMP), Beckman Laser Institute and Medical Clinic,^{*} Department of Physiology and Biophysics,[†] Department of Chemistry,^{**} and Department of Biomedical Engineering,^{††} University of California, Irvine, CA; and Division of Renal Diseases and Hypertension,[§] Department of Medicine, University of Colorado, Denver, CO

Abstract We characterized several cellular and structural features of early stage Type II/III atherosclerotic plaques in an established model of atherosclerosis—the ApoE-deficient mouse—by using a multimodal, coregistered imaging system that integrates three nonlinear optical microscopy (NLOM) contrast mechanisms: coherent anti-Stokes Raman scattering (CARS), second harmonic generation (SHG), and two-photon excitation fluorescence (TPEF). Specifically, the infiltration of lipid-rich macrophages and the structural organization of collagen and elastin fibers were visualized by CARS, SHG, and TPEF, respectively, in thick tissue specimens without the use of exogenous labels or dyes. Label-free CARS imaging of macrophage accumulation was confirmed by histopathology using CD68 staining. A high-fat, high-cholesterol Western diet resulted in an approximate 2-fold increase in intimal plaque area, defined by CARS signals of lipid-rich macrophages. Additionally, analysis of collagen distribution within lipid-rich plaque regions revealed nearly a 4-fold decrease in the Western diet-fed mice, suggesting NLOM sensitivity to increased matrix metalloproteinase (MMP) activity and decreased smooth muscle cell (SMC) accumulation. These imaging results provide significant insight into the structure and composition of early stage Type II/III plaque during formation and allow for quantitative measurements of the impact of diet and other factors on critical plaque and arterial wall features.—Lim, R. S., A. Kratzer, N. P. Barry, S. Miyazaki-Anzai, M. Miyazaki, W. W. Mantulin, M. Levi, E. O. Potma, and B. J. Tromberg. Multimodal CARS microscopy determination of

the impact of diet on macrophage infiltration and lipid accumulation on plaque formation in ApoE-deficient mice. *J. Lipid Res.* 2010. 51: 1729–1737.

Supplementary key words atherosclerosis • extracellular matrix • collagen • elastin • arteries • nonlinear optical microscopy

Atherosclerosis is a progressive disease that is characterized by the accumulation of lipids, monocytes, fibrous constituents, and various other inflammatory cells in the arterial wall. These deposits form vascular lesions known as atheromatous plaques, which contain necrotic cores and are separated from the arterial intima by a fibrous cap made up of collagen and smooth muscle cells (1, 2). As these plaques grow with time, their fibrous caps become thin and increasingly susceptible to tearing, thus becoming more vulnerable to rupture. Rupture of these vulnerable plaques releases the inflammatory elements of the necrotic core into the artery, causing thrombosis. This leakage subsequently leads to obstruction of arterial blood flow and, possibly, angina and/or myocardial infarction (3).

As the single most important contributor to cardiovascular disease-related deaths, atherosclerosis serves as a significant topic for scientific research, specifically in terms of diagnosis and prevention. Unfortunately, although con-

This study was supported by National Institutes of Health Grants DK-066029, DK-076134, AG-026529, Abbott, and VA (M.L.); and National Institutes of Health Grant P41-RR01192 (LAMMP); by National Science Foundation Grant DBI-0754624 (E.O.P.); by the Beckman Foundation; and by Air Force Office of Scientific Research Grant FA9550-08-1-0384 (B.J.T.). Its contents are solely the responsibility of the authors and do not necessarily represent the official views of the National Institutes of Health or other granting agencies.

Manuscript received 4 November 2009 and in revised form 5 March 2010.

*Published, JLR Papers in Press, March 5, 2010
DOI 10.1194/jlr.M003616*

Abbreviations: Apo, apolipoprotein; BCA, brachiocephalic; CARS, coherent anti-Stokes Raman scattering; MMP, matrix metalloproteinase; NLOM, nonlinear optical microscopy; OCT, optical coherence tomography; PMT, photomultiplier tube; SHG, second harmonic generation; SMC, smooth muscle cell; TPEF, two-photon excitation fluorescence.

¹To whom correspondence should be addressed.

e-mail: bjtrombe@uci.edu

[§]The online version of this article (available at <http://www.jlr.org>) contains supplementary data in the form of four movies.

siderable efforts have been made to detect atherosclerosis and characterize vulnerable plaque, it is still difficult to detect plaque formation at its earliest stages of development. This complication is due to its asymptomatic nature, as vulnerable plaques grow without causing any detrimental side effects until rupture (1). Current arterial imaging techniques that are being used in the clinical setting provide information only at later stages of the disease process (e.g., stenosis and thrombus formation, by angiography and angioscopy, respectively) or produce limited information about the vessel wall and general tissue structure (e.g., intima-media thickness and presence of lipid-rich tissue, by ultrasound and magnetic resonance imaging, respectively) (4–8). Although these techniques provide insight into the disease state, they are incapable of cellular-level resolution and typically require the addition of exogenous contrast agents (4, 9–12).

To overcome the inherent limitations of these methods, label-free imaging modalities have been explored and are currently being developed by several groups. Clinically, some of these techniques include intravascular optical coherence tomography (OCT) and near-infrared reflectance spectroscopy (9, 13–18). These methods, which provide significantly improved information about plaque structure and composition, are currently under investigation in large-scale clinical studies (19, 20).

Nonlinear multimodal microscopy provides a similarly label-free strategy for visualizing key tissue components and biochemical composition, but at submicron resolution and with highly specific chemical identification (21–23). Using a multimodal platform, selective imaging of tissue collagen, elastin, and lipids is achieved with second harmonic generation (SHG), two-photon excited fluorescence (TPEF), and coherent anti-Stokes Raman scattering (CARS), respectively. The selective imaging capabilities and high resolution make nonlinear microscopy an attractive imaging approach for studying and detecting atherosclerosis, particularly in small animal models and basic research studies.

In previous work, nonlinear microscopy, using combined SHG and TPEF imaging, was shown to reveal structural collagen and elastin fibers of the extracellular matrix in the arterial wall, the site of atherosclerotic plaque development (4, 12, 24, 25). In addition, Wang et al. demonstrated that SHG/TPEF/CARS imaging can be used to identify endothelial and smooth muscle cells in the arterial wall (26). Using an Ossabaw swine model, Le et al. showed that nonlinear microscopy enables a detailed study of atherosclerotic plaques, including the visualization of extra-cellular lipids and lipid-rich cells associated with plaque lesions (27). The ability to probe both the structural proteins of the arterial wall and the accumulation of lipid within atherosclerotic regions makes nonlinear imaging suitable for quantitative analysis of disease progression. Wang et al. have used this quantitative capability to determine lipid concentration levels in various lesions of pathological intima (28).

To take full advantage of the inherent capabilities of nonlinear optical microscopy, it is important to evaluate the technique when applied to the apolipoprotein E-deficient ($ApoE^{-/-}$) mouse model, an established and versa-

tile model for atherosclerotic disease (12, 29–32). The $ApoE^{-/-}$ model offers many advantages in terms of transgenic flexibility. Carotid arteries of $ApoE^{-/-}$ mice in vivo have recently been imaged successfully in a nonlinear optical microscope. Yu et al. resolved elastin autofluorescence and collagen SHG of the carotid arterial tissue of the $ApoE^{-/-}$ model, and identified lipid and endothelial cells using fluorescent labels (33).

In this work, we further develop nonlinear multimodal imaging as an imaging tool for atherosclerotic research. Whereas lipids in the $ApoE^{-/-}$ model were previously probed with the aid of fluorescent markers (33), here we aim to examine the mouse model using CARS contrast for lipid identification. Using an en face imaging geometry, complete sections of brachiocephalic arteries are examined, revealing lipid-rich macrophages in plaque lesions and collagen/elastin fibers in the arterial wall. Having established these contrast parameters, we study differences in atherosclerotic plaques based on diet. Mice were fed either a standard low-fat diet or a high-fat, high-cholesterol Western diet to accelerate disease progression. Our imaging results show a clear diet dependence of atherosclerotic lesions in terms of lesion size, macrophage and lipid density, and collagen content. Specifically, in the Western diet group, quantitative arterial imaging reveals an approximate 2-fold increase in intimal plaque area, defined by lipid-rich macrophage accumulation, as well as a nearly 4-fold decrease in collagen distribution within those lipid-rich plaque regions.

MATERIALS AND METHODS

Atherosclerotic ApoE-deficient mouse model

Previous studies have shown that the apolipoprotein E gene knockout ($ApoE^{-/-}$) mouse suffers from delayed clearance of lipoproteins, thus causing the development of fatty streaks and widespread fibrous plaques at vascular sites that are typically affected in human atherosclerosis (29–32). In this study, male $ApoE^{-/-}$ mice on a C57BL/6 background were received from Jackson laboratory (Bar Harbor, ME). Mice were fed either a Western-type diet (TD.07730 containing 21% fat and 0.2% cholesterol) or a control, low-fat diet (TD.07731 containing 4% fat and 0.02% cholesterol), which were both adjusted in calcium and magnesium content (1.2% calcium, 0.25% magnesium). Both diets were obtained from Harlan Teklad, USA. Standard C57BL/6 (non- $ApoE^{-/-}$) mice fed the control, low-fat diet and the Western-type diet were also used as negative controls in our quantitative studies. Mice were maintained in a clean environment on a regular light-dark cycle (12 h light, 12 h dark). Before the initiation of the corresponding diets, mice were kept on a standard laboratory diet (2018 Teklad Global 18% protein rodent diet) for 1 week. After 19–20 weeks mice were anesthetized with phenobarbital (100 μ l per mouse). Each animal was perfused with 10ml 1 \times PBS by applying heart puncture with a butterfly needle (23-gauge 3/4). After the animal was perfused free of all blood, the tissues were fixed by perfusing with 2% 10–20 ml freshly prepared PFA (in 1 \times PBS). The aortas and the brachiocephalic arteries (BCA) were postfixed in fresh 2% PFA for 24 h. Thereafter, the BCA were stored and preserved in 1 \times PBS supplemented with sodium azide for imaging. Animal experiments were approved by the Institutional Animal Care and Use Committee (IACUC) at the University of Colorado, Denver.

Immunohistochemistry. To confirm the presence of macrophage cells within the arterial wall, 5- μm thick sections of the aortic arch from standard, low-fat diet-fed ApoE^{-/-} mice and Western diet-fed ApoE^{-/-} mice were processed, cut, and prepared for immunohistochemical analysis. Briefly, sections were incubated with 0.5% Triton X-100 for 2 min at room temperature and then washed twice with PBS. To block nonspecific binding of the primary antibody, a 3% BSA dilution in PBS was used for 60 min at room temperature. Sections were incubated with a 1:300 dilution in blocking solution of rat monoclonal antibody to mouse macrosialin, the murine homolog of the human macrophage glycoprotein CD68 (MCA1957; AbD Serotec, Raleigh, NC), for 60 min at room temperature. After washing with blocking solution, slides were then incubated with a 1:300 dilution in blocking solution of Alexa Fluor 488 donkey anti-rat immunoglobulins (A-21208; Invitrogen, Carlsbad, CA) for 60 min at room temperature. Slides were then washed with PBS, dried, and mounted with Aqua-Mount aqueous mounting medium (13800; Lerner Laboratories, Pittsburgh, PA).

Sample handling. We imaged ~ 10 mm-long regions of the brachiocephalic artery (~ 150 mm²) in ApoE-deficient mice fed either a standard low-fat diet or a high-fat, high-cholesterol Western diet, which is known to accelerate the disease process (30, 31). To visualize the lesions from the arterial intima out toward the adventitia, the aortas were sliced longitudinally and laid out en face onto a glass coverslip, with the luminal side face-down and closest to the objective lens of the inverted microscope (Fig. 1). A second coverslip was placed on top of the artery and secured along two opposite edges with an epoxy resin to prevent motional artifacts and to keep the luminal surface in contact with the bottom coverslip. The non-secured edges allowed for the addition of PBS to keep the tissue from drying out.

Nonlinear optical imaging. The pump and Stokes beams required for the CARS process were derived from a synchronously pumped optical parametric oscillator system. The 1064-nm, 7-ps pulses of a 76 MHz mode-locked Nd:vanadate laser source (High-Q, Hohenems, Austria) provided the Stokes radiation. A portion of the same 1064-nm source was used to pump an optical parametric oscillator (Levante, Berlin, Germany), tunable in the 760–960 nm range, which delivered the pump beam for the CARS process. The frequency difference between the pump and the Stokes radiation was set to 2852 cm⁻¹, corresponding to the symmetric CH₂ vibration of lipid. For the reported experiments, the pump beam was set to 816.3 nm. In addition, the 816.3 nm radiation also served as the driving beam for the SHG process. The collinearly overlapped pump and Stokes beams were passed through a laser scanner (Fluoview 300, Olympus, Center Valley, PA.) and focused with a 20 \times UPLAPO objective (Olympus) into the sample. The average power at the sample was ~ 10 mW for the Stokes beam and 20 mW for the pump beam.

The inverted microscope (IX71 Olympus) is equipped with three photomultiplier tubes (PMT). In the forward direction, the SHG

and CARS light were captured by a condenser lens (0.55 NA) and directed to a 760-nm long-wave pass dichroic mirror (z760xrdc, Chroma, Rockingham, VT). The reflected light was passed on to a dichroic mirror (FM02, Thorlabs, Newton, NJ) for separating the SHG and forward (F-) CARS signals. The CARS detector consists of two 650 \pm 40 nm bandpass filters (HQ650/40, Chroma) and a red-sensitive PMT, while the SHG detector includes a set of two 400 \pm 40 nm bandpass filters and a PMT photodetector. In the backward (epi-) direction, TPEF radiation was reflected off a 760 nm long-pass dichroic mirror, passed through a 550 \pm 20 nm bandpass filter, and sent onto a PMT. All nonlinear signals were detected by red-sensitive PMTs (R3896, Hamamatsu, Hamamatsu City, Japan). Total acquisition time for each image was 4.96 s per scan, with each image integrated over three averages. Single-plane XY images and multiplane XYZ image stacks were taken, as well as XZ cross-sectional scans.

Once collected, images were processed using ImageJ imaging software for quantitative analysis. For composite arterial images, several individual image tiles (512 \times 512 pixels²) were cropped and manually stitched together (approximately 8 \times 10 tiles per full image) to recreate the full view of the artery.

RESULTS

En face multimodal imaging identifies lipid-rich regions within Type II and III plaque lesions

Representative images of the entire artery for both standard and Western diets are shown in Figs. 2 and 3. The TPEF (green) and SHG (blue) channels clearly reveal the elastin structure throughout the tissue and distinct regions of collagen fiber accumulation, respectively. The CARS (red) channel shows significant aggregates of lipid at several locations along the artery, indicating atherosclerotic plaque lesions. Individual tile images and multiplane image stacks of a second set of arteries, fed the same standard or Western diet (Fig. 4 and supplementary movies I, II), as well as XZ cross-sectional images (Fig. 5 and supplementary movies III, IV) provide more in-depth views of these lipid-rich regions, subsequently revealing the organization of elastin, collagen, and lipids. In these images, specifically in the XZ cross-sections, the lesions appear to be characterized by lipid droplets embedded in a network of elastin fibers closest to the arterial lumen. A distinct layer of collagen surrounds the lipids closer to the adventitial surface.

The plaque lesions observed in both standard diet-fed and Western diet-fed mice predominantly correspond to Type II and III early atherosclerotic plaques (Fig. 6). Most lesions are characterized by intracellular lipid accumulation with very few quantities of thinly dispersed lipid drop-

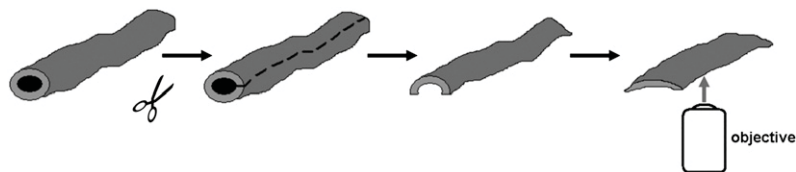


Fig. 1. Schematic of aortic tissue preparation for en face imaging. Tissue samples were cut once along the length of the artery and laid flat between two glass coverslips. The luminal side was placed face-down on the stage of the inverted microscope so that the imaging orientation was consistently directed from the intimal layer out to the adventitial surface. Total tissue surface area was approximately 150 mm².

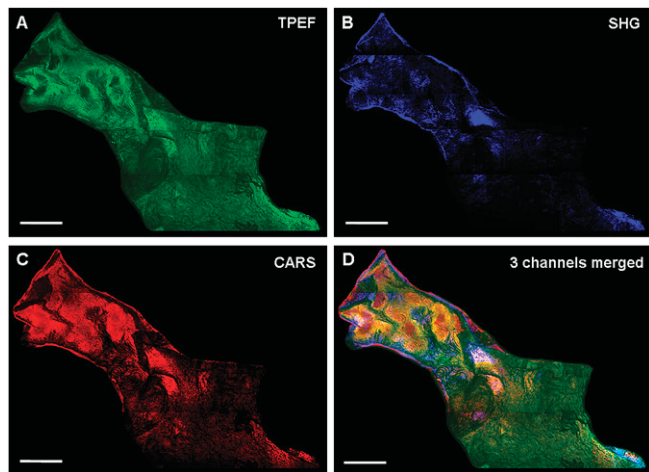


Fig. 2. Representative composite images of the entire descending aorta in ApoE-deficient mice fed a standard low-fat diet. Images from three separate channels—TPEF (A), SHG (B), and CARS (C)—were acquired simultaneously, with all three channels visible in D. Each image consists of several individual image tiles, cropped and stitched together (approximately 8×10 tiles per composite image). Scale bar, lower left of each image = 500 μm . CARS, coherent anti-Stokes Raman scattering; SHG, second harmonic generation; TPEF, two-photon excitation fluorescence.

lets and vesicular particles within the extracellular space, which is indicative of Type II lesions (34, 35). These observations are consistent with studies in other laboratory animals, where Type II lesions are most readily produced. However, in the Western diet-fed mice, the extracellular lipid droplets and particles become more prevalent, as they begin to form small lipid pools which will eventually become the foundation of the atheromatous lipid core (35, 36). These observations indicate the early presence of Type III plaque lesions.

These results confirm that nonlinear multimodal imaging is highly sensitive to several unique features of the plaque lesion and therefore provides a highly capable means of plaque detection in the en face geometry.

CARS imaging identifies macrophages

Although the gross surrounding architecture and organization of components within the lesion are readily identified with nonlinear multimodal microscopy, more specific information is attained when examining structures at the cellular level. During the early stages of atherosclerosis, monocytes are recruited to the arterial endothelium as part of the body's natural immune response to the onset of disease. These monocytes differentiate into macrophage cells, become filled with fat, lipids, and various inflammatory elements, and eventually grow until rupture, thus defining the atherosclerotic plaque. High-magnification CARS images ($40\times$) at various levels of electronic optical zoom (2–6.5 times the original image) reveal distinct cellular structures that morphologically resemble macrophage cells, in both standard diet-fed and Western diet-fed mice (Fig. 7). These structures have well-defined nuclei and exhibit strong CARS signals, indicating the abundance of lipids in cytosolic parts of the cells. To con-

firm identification of these cellular structures as macrophage cells, immunohistochemical analysis was performed using a primary antibody against mouse macrophage glycoprotein CD68. The coregistered CARS/TPEF immunofluorescence images confirm that these structures are macrophages (Fig. 8).

Plaque lesions exhibit an increase in overall lipid content in Western diet-fed mice

We performed a quantitative analysis of the images to acquire insight into the biochemical and structural changes that occur during disease progression. We specifically focused on the relative changes in lipid levels between the standard diet-fed atherosclerotic mice and the Western diet-fed, accelerated disease state mice. To determine these changes, we measured lipid accumulation within plaque lesions. Using ImageJ imaging software, we first defined lipid-rich plaque regions by determining a threshold based on lipid signal intensity in the CARS channel (histograms not shown) and then measured only the regions above the threshold value in our analysis of lipid area. Total tissue surface area ($\sim 150 \text{ mm}^2$) was measured with the threshold set to 1 (out of a maximum of 255) to exclude the background. Total plaque lesion area was then defined as the ratio of lipid area to total tissue area.

In the standard diet-fed mice, lipid accumulation occupied approximately 11% (11.21 ± 2.58) of the entire artery, on average ($n = 4$) (Fig. 9). In contrast, the Western diet-fed mice displayed an average lipid occupation of 22%

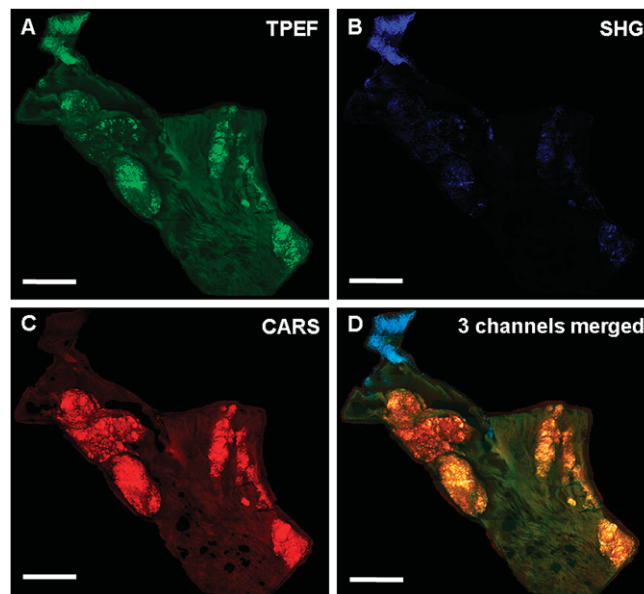


Fig. 3. Representative composite images of the entire descending aorta in ApoE-deficient mice fed a Western diet. Images from three separate channels—TPEF (A), SHG (B), and CARS (C)—were acquired simultaneously, with all three channels visible in D. Each image consists of several individual image tiles, cropped and stitched together (approximately 8×10 tiles per composite image). Scale bar, lower left of each image = 500 μm . CARS, coherent anti-Stokes Raman scattering; SHG, second harmonic generation; TPEF, two-photon excitation fluorescence.

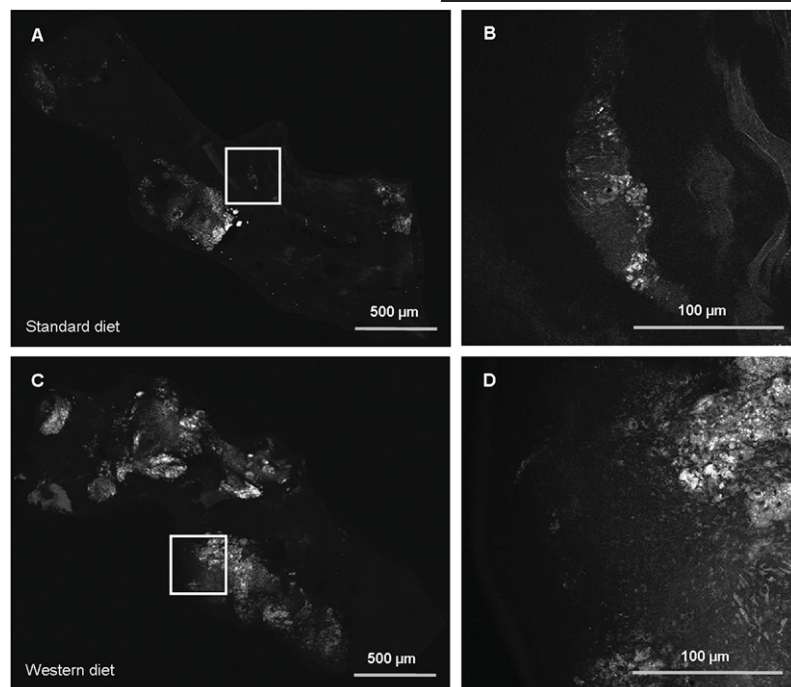


Fig. 4. CARS composite images of the entire descending aorta in ApoE-deficient mice fed either a standard low-fat diet or a Western diet, with specific regions of lipid accumulation highlighted. Enlarged images (B and D) to the right of composite images (A and C) represent uncropped, single-image tiles at full magnification (20 \times) of the regions highlighted in A and C. Distinct lipid deposits and collagen fibers are evident. Corresponding scale bars are located at the lower right of each image. Apo, apolipoprotein.

(22.22 ± 3.43), which signifies a roughly 2-fold increase in overall lipid abundance (and therefore, overall lesion area) between the two diets. Lipid accumulation was also measured in both standard diet-fed and Western diet-fed C57BL/6 non-ApoE^{-/-} mice as negative controls. To ensure that the lipid-abundant lesions were similar between the two diets, we measured the lipid intensity profile based on the overall lipid signal intensity (**Fig. 10**). The signal intensity remained relatively constant between the two diets (94.13 ± 1.80 in standard diet versus 89.36 ± 2.95 in Western diet, on a 0–255 scale), suggesting that there was no difference in the lipid concentration in the different plaques.

Collagen content decreases within plaque lesions and in the surrounding structural matrix

In addition to analyzing the biochemical composition of the plaque lesion, we also quantitatively characterized and measured the structural changes that occur at lesion sites and within the surrounding matrix of the vessel wall. Specifically, we measured the amount of collagen both within and around the plaque. For our measurements of collagen distribution within the plaque lesion, we first separated

the signal of the SHG channel from the previously defined CARS-based images of lipid-rich plaque regions (which we determined with a CARS-based signal threshold). These SHG-based images subsequently featured only collagen within the lipid-rich plaque regions. We measured the collagen with an SHG signal threshold set to 1 (out of a maximum of 255) to include all collagen within the plaques and to exclude only the background. Colocalization of collagen and lipids was then defined as the ratio of total collagen content within the lipid-rich plaque regions to the lipid area determined previously with the CARS-based threshold value. For our measurements of collagen in the surrounding matrix structure (i.e., collagen not associated with lipid-rich plaque regions), we followed an approach similar to our previous analysis. However, instead of separating the SHG signal from the lipid-rich plaque images that were determined with a CARS-based signal threshold, we separated the SHG signal from the raw, multichannel images, thereby maintaining signal from all of the collagen within the tissue. We then subtracted the plaque-associated collagen signal from the total tissue collagen signal to obtain only the non-lipid-associated collagen.

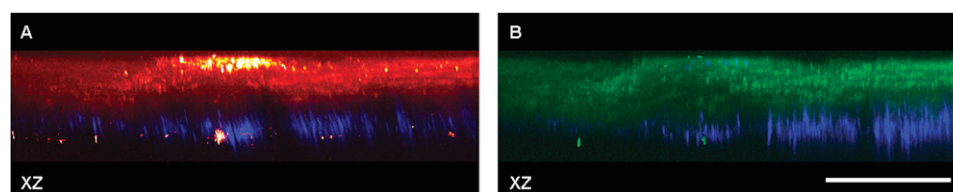


Fig. 5. XZ cross-sectional images of lipid-rich region in the standard diet mouse of Figure 4. CARS/SHG (A) and TPEF/SHG (B) images were taken separately to facilitate visualization of unique structures corresponding to signal origin (i.e., lipid deposits from red CARS, collagen structure from blue SHG, and elastin fibers from green TPEF). Scale bar, lower right = 200 μ m. CARS, coherent anti-Stokes Raman scattering; SHG, second harmonic generation; TPEF, two-photon excitation fluorescence.

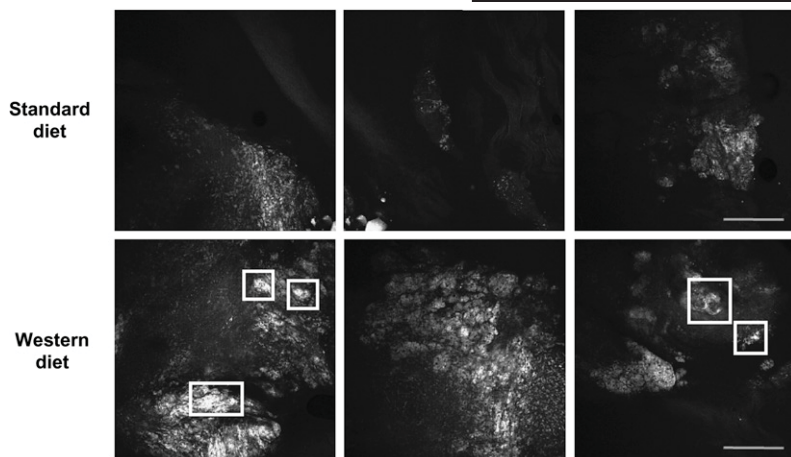


Fig. 6. CARS images of type II and III plaque lesions within standard diet–fed and Western diet–fed atherosclerotic ApoE-deficient mice. Lesions are mostly characterized by intracellular lipid accumulation within macrophage cells, which is indicative of Type II lesions. However, in the Western diet–fed mice, some small pools of extracellular lipids are also evident (highlighted with boxes), indicating Type III lesions. Scale bar, lower right = 100 μ m. Apo, apolipoprotein; CARS, coherent anti-Stokes Raman scattering.

Analysis of collagen structure distribution within the plaque lesions revealed a significant change, as the Western diet–fed mice displayed nearly a 4-fold decrease in the amount of collagen that colocalized with plaque-associated lipids ($12.76\% \pm 6.44$ in standard diet versus $3.61\% \pm 0.11$ in Western diet) (**Fig. 11**). Collagen content in the surrounding matrix also decreased in a similar fashion ($6.57\% \pm 0.37$ in standard diet versus $2.49\% \pm 0.88$ in Western diet). These biochemical and structural changes suggest a strong correlation between plaque development and dietary conditions, and therefore suggest the potential for such changes as useful markers for early plaque detection.

DISCUSSION

The goal of this study was to determine the capability of coregistered nonlinear optical microscopy (NLOM) signals (CARS, SHG, and TPEF) to detect early stage Type II and III plaque formation. Specifically, we were able to identify and characterize lipid-rich macrophage cells within the plaque interior and measure the increase in overall lipid plaque area in the Western diet–fed, accelerated disease state, ApoE-deficient mouse. We also visualized the collagen- and elastin-rich extracellular matrix

structure of the aortic vessel wall, within and around the plaque lesions. The covisualization of elastin and lipid in our CARS images aids in identifying plaque regions. Consequently, we were able to quantitatively measure the decrease in overall collagen content in the plaques of the Western diet–fed mouse.

A major finding of this study is an increase in overall lipid accumulation within the plaque lesions of the Western diet–fed ApoE-deficient mouse. Previous studies in other animal models have shown similar trends of increased lipid accumulation within various lesion types of atherosclerotic plaque (26–28). However, the work presented here marks the first report of multimodal CARS imaging of increased lipid accumulation as a function of dietary conditions (Figs. 2–8). The use of CARS microscopy for selective detection of lipids in atherosclerotic tissue presents several significant advantages over existing optical techniques used for determining lipid content in

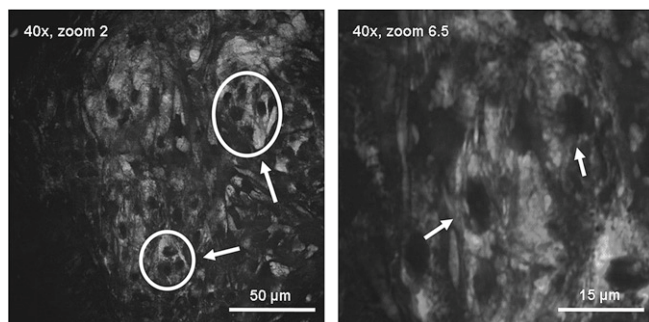


Fig. 7. Representative CARS images of macrophage-like cellular structures within plaque lesions, at 40 \times magnification and two different levels of electronic optical zoom. Clusters of macrophage cells, defined by dark nuclei, are indicated by arrows. Corresponding scale bars are located at the lower right of each image. CARS, coherent anti-Stokes Raman scattering.

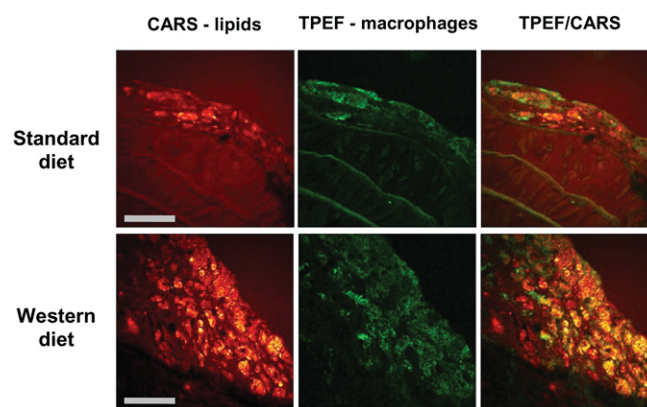


Fig. 8. Images of macrophage cells in atheromatous plaque lesions obtained from simultaneously acquired CARS and TPEF signals. On the left, CARS (red) images of lipids from standard (upper) and western (lower) diet animals. In the middle, TPEF (green) images of CD68-stained, immunofluorescent (Alexafluor 488) macrophage cells from standard (upper) and western (lower) diet animals. On the right, coregistered CARS and TPEF shows colocalization of lipid and CD68, respectively, confirming CARS identification of macrophage cells in plaques. Scale bar, lower left = 200 μ m. CARS, coherent anti-Stokes Raman scattering; TPEF, two-photon excitation fluorescence.

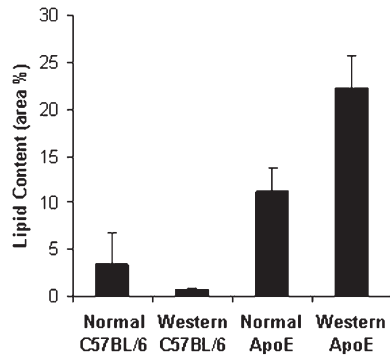


Fig. 9. Lipid accumulation in the arterial wall of standard diet-fed and Western diet-fed ApoE-deficient mice. Total lipid content is defined as the ratio of lipid area to total tissue area. Normal C57BL/6 mice (non-ApoE^{-/-}) fed a standard diet and a Western diet were included as negative controls. Apo, apolipoprotein.

tissues. Compared with infrared spectroscopic approaches, CARS offers subcellular resolution and optical sectioning, which enable the identification of individual macrophages and provide a clear depth-resolved picture of the lesion in the blood vessel wall. Alternative techniques based on fluorescent stains, such as Oil-Red-O, are unattractive for in vivo imaging and are known to produce tentative artifacts that may affect the quantitative analysis (37). Importantly, the label-free detection of lipids provided by CARS can be combined with endoscopic probing, opening the door for in vivo optical examination of intravascular lesions. Recently, significant progress has been made with integrating nonlinear optical modalities, such as SHG and CARS, in a fiber-based probe (38), underscoring the potential of the nonlinear imaging approach for research of cardiovascular disease.

While lipid accumulation increased in the Western diet-fed mice, the amount of collagen within the plaque lesions decreased (Fig. 11). Several mechanisms may account for this observation. Shah et al. demonstrated that macrophages induce collagen breakdown in the fibrous caps of atherosclerotic plaques, and the addition of a matrix metalloproteinase (MMP) inhibitor partially blocks this process (39). Aikawa et al. further reported that lipid lowering by diet stabilizes atherosclerotic plaques by reducing

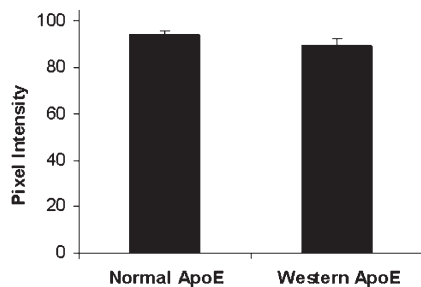


Fig. 10. General intensity profile of atheromatous plaque lesions in the arterial wall of standard diet-fed and Western diet-fed ApoE-deficient mice. Lesion profile is defined by the overall CARS signal intensity from lipids within the plaque lesion. Apo, apolipoprotein; CARS, coherent anti-Stokes Raman scattering.

both lipid accumulation and proteolytic enzyme activity, specifically interstitial collagen degradation by MMP-1, MMP-2, MMP-3, and MMP-9 (40). These findings directly suggest a significant role for MMPs in the integrity of the atherosclerotic plaque and also confirm the dependence of MMP activity on lipid-based dietary conditions. In a separate study, Aikawa et al. also showed that dietary lipid lowering promotes the accumulation of mature smooth muscle cells (SMC) in atheroma (41). SMCs provide the cellular source of collagen fibers within the arterial wall, and therefore, an increase in SMC accumulation would directly promote collagen formation at plaque lesions. The decrease in collagen content that we observed in the Western diet-fed ApoE-deficient mice may therefore be attributed to a combination of increased MMP activity and decreased SMC accumulation at lesion sites. Dietary conditions did not, however, produce an impact on elastin distribution within the tissue. Further investigation into the specific roles of both MMPs and SMCs in the maintenance of plaque structure is necessary.

CONCLUSION

We employed high-resolution, multimodal nonlinear optical microscopy (NLOM) for quantitative analysis of complete brachiocephalic arteries (~150 mm²) in ApoE-deficient mice. Specifically, lipid, collagen, and elastin were detected by CARS, SHG, and TPEF intrinsic signals, respectively, in thick tissue specimens without the use of exogenous labels. Our results reveal significant changes that occur both in the cellular composition of the plaque lesions and the surrounding structure of the extracellular matrix. A high-fat, high-cholesterol Western diet resulted in elevated lipid and macrophage content and reduced collagen in plaques and the surrounding arterial wall. These observations are consistent with known mechanisms of Type II/III atherosclerotic lesion formation, and NLOM identification of macrophage cells was confirmed by histopathology. Future investigations may involve manipulating nondietary factors, such as chronic renal failure, which

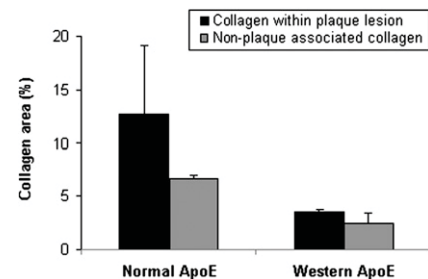



Fig. 11. Collagen distribution within plaque lesions and in the surrounding structural matrix of standard diet-fed and Western diet-fed ApoE-deficient mice. Colocalization of collagen and lipids within the plaque lesion (i.e., plaque-associated collagen area) is defined as the ratio of total collagen content within lipid-rich plaque regions to the total area of those lipid regions. Nonplaque-associated collagen is defined as the ratio of nonplaque-associated collagen area to total tissue area. Apo, apolipoprotein.

has previously been linked to accelerated atherosclerosis and arterial calcification and has high clinical relevance (29, 42, 43). Overall, multimodal NLOM has exceptional sensitivity to vascular wall structures. It is a promising approach for quantifying the early appearance and progression of plaque formation and is expected to become an important new tool for atherosclerosis research. 

REFERENCES

- Narula, J., and H. W. Strauss. 2005. Imaging of unstable atherosclerotic lesions. *Eur. J. Nucl. Med. Mol. Imaging* **32**: 1–5.
- Virmani, R., F. D. Kolodgie, A. P. Burke, A. V. Finn, H. K. Gold, T. N. Tulenko, S. P. Wrenn, and J. Narula. 2005. Atherosclerotic plaque progression and vulnerability to rupture: angiogenesis as a source of intraplaque hemorrhage. *Arterioscler. Thromb. Vasc. Biol.* **25**: 2054–2061.
- Marcu, L., Q. Fang, J. A. Jo, T. Papaioannou, A. Dorafshar, T. Reil, J. H. Qiao, J. D. Baker, J. A. Freischlag, and M. C. Fishbein. 2005. In vivo detection of macrophages in a rabbit atherosclerotic model by time-resolved laser-induced fluorescence spectroscopy. *Atherosclerosis* **181**: 295–303.
- Waxman, S., F. Ishibashi, and J. E. Muller. 2006. Detection and treatment of vulnerable plaques and vulnerable patients: novel approaches to prevention of coronary events. *Circulation* **114**: 2390–2411.
- Kaufmann, B. A., and J. R. Lindner. 2007. Molecular imaging with targeted contrast ultrasound. *Curr. Opin. Biotechnol.* **18**: 11–16.
- Amirbekian, V., M. J. Lipinski, K. C. Briley-Saebo, S. Amirbekian, J. G. Aguinaldo, D. B. Weinreb, E. Vucic, J. C. Frias, F. Hyafil, V. Mani, et al. 2007. Detecting and assessing macrophages in vivo to evaluate atherosclerosis noninvasively using molecular MRI. *Proc. Natl. Acad. Sci. USA* **104**: 961–966.
- Frias, J. C., M. J. Lipinski, S. E. Lipinski, and M. T. Albelda. 2007. Modified lipoproteins as contrast agents for imaging of atherosclerosis. *Contrast Media Mol. Imaging* **2**: 16–23.
- Sirol, M., V. Fuster, and Z. A. Fayad. 2006. Plaque imaging and characterization using magnetic resonance imaging: towards molecular assessment. *Curr. Mol. Med.* **6**: 541–548.
- Arakawa, K., K. Isoda, T. Ito, K. Nakajima, T. Shibuya, and F. Ohsuzu. 2002. Fluorescence analysis of biochemical constituents identifies atherosclerotic plaque with a thin fibrous cap. *Arterioscler. Thromb. Vasc. Biol.* **22**: 1002–1007.
- Lipinski, M. J., J. C. Frias, and Z. A. Fayad. 2006. Advances in detection and characterization of atherosclerosis using contrast agents targeting the macrophage. *J. Nucl. Cardiol.* **13**: 699–709.
- Lipinski, M. J., V. Amirbekian, J. C. Frias, J. G. Aguinaldo, V. Mani, K. C. Briley-Saebo, V. Fuster, J. T. Fallon, E. A. Fisher, and Z. A. Fayad. 2006. MRI to detect atherosclerosis with gadolinium-containing immunomicelles targeting the macrophage scavenger receptor. *Magn. Reson. Med.* **56**: 601–610.
- van Zandvoort, M., W. Engels, K. Douma, L. Beckers, M. Oude Egbrink, M. Daemen, and D. W. Slaaf. 2004. Two-photon microscopy for imaging of the (atherosclerotic) vascular wall: a proof of concept study. *J. Vasc. Res.* **41**: 54–63.
- Cilingiroglu, M., J. H. Oh, B. Sugunan B, N. J. Kemp, J. Kim, S. Lee, H. N. Zaatari, D. Escobedo, S. Thomsen, T. E. Milner, et al. 2006. Detection of vulnerable plaque in a murine model of atherosclerosis with optical coherence tomography. *Catheter. Cardiovasc. Interv.* **67**: 915–923.
- Tearney, G. J., I. K. Jang, and B. E. Bouma. 2006. Optical coherence tomography for imaging the vulnerable plaque. *J. Biomed. Opt.* **11**: 021002.
- Christov, A., R. M. Korol, E. Dai, L. Liu, H. Guan, M. A. Bernards, P. B. Cavers, D. Susko, and A. Lucas. 2005. In vivo optical analysis of quantitative changes in collagen and elastin during arterial remodeling. *Photochem. Photobiol.* **81**: 457–466.
- Lembcke, A. 2007. Coronary artery calcifications: a critical assessment of imaging techniques. *Blood Purif.* **25**: 115–119.
- Pande, A. N., R. H. Kohler, E. Aikawa, R. Weissleder, and F. A. Jaffer. 2006. Detection of macrophage activity in atherosclerosis in vivo using multichannel, high-resolution laser scanning fluorescence microscopy. *J. Biomed. Opt.* **11**: 021009.
- Wang, J., Y. J. Geng, B. Guo, T. Klima, B. N. Lal, J. T. Willerson, and W. Casscells. 2002. Near-infrared spectroscopic characterization of human advanced atherosclerotic plaques. *J. Am. Coll. Cardiol.* **39**: 1305–1313.
- Kashiwagi, M., A. Tanaka, H. Kitabata, H. Tsujioka, H. Matsumoto, Y. Arita, K. Ookochi, A. Kuroi, H. Kataiwa, T. Tanimoto, et al. 2009. Relationship between coronary arterial remodeling, fibrous cap thickness and high-sensitivity C-reactive protein levels in patients with acute coronary syndrome. *Circ. J.* **73**: 1291–1295.
- Moreno, P. R., R. A. Lodder, K. R. Purushothaman, W. E. Charash, W. N. O'Connor, and J. E. Muller. 2002. Detection of lipid pool, thin fibrous cap, and inflammatory cells in human aortic atherosclerotic plaques by near-infrared spectroscopy. *Circulation* **105**: 923–927.
- Campagnola, P. J., A. C. Millard, M. Terasaki, P. E. Hoppe, C. J. Malone, and W. A. Mohler. 2002. Three-dimensional high-resolution second-harmonic generation imaging of endogenous structural proteins in biological tissues. *Biophys. J.* **82**: 493–508.
- Zoumi, A., A. Yeh, and B. J. Tromberg. 2002. Imaging cells and extracellular matrix in vivo by using second-harmonic generation and two-photon excited fluorescence. *Proc. Natl. Acad. Sci. USA* **99**: 11014–11019.
- Rodriguez, L. G., S. J. Lockett, and G. R. Holtom. 2006. Coherent anti-stokes Raman scattering microscopy: a biological review. *Cytometry A* **69**: 779–791.
- Lilledahl, M. B., O. A. Haugen, C. de Lange Davies, and L. O. Svaasand. 2007. Characterization of vulnerable plaques by multiphoton microscopy. *J. Biomed. Opt.* **12**: 044005.
- Zoumi, A., X. Lu, G. S. Kassab, and B. J. Tromberg. 2004. Imaging coronary artery microstructure using second-harmonic and two-photon fluorescence microscopy. *Biophys. J.* **87**: 2778–2786.
- Wang, H. W., T. T. Le, and J. X. Cheng. 2008. Label-free imaging of arterial cells and extracellular matrix using a multimodal CARS microscope. *Opt. Commun.* **281**: 1813–1822.
- Le, T. T., I. M. Langohr, M. J. Locker, M. Sturek, and J. X. Cheng. 2007. Label-free molecular imaging of atherosclerotic lesions using multimodal nonlinear optical microscopy. *J. Biomed. Opt.* **12**: 054007.
- Wang, H. W., I. M. Langohr, M. Sturek, and J. X. Cheng. 2009. Imaging and quantitative analysis of atherosclerotic lesions by CARS-based multimodal nonlinear optical microscopy. *Arterioscler. Thromb. Vasc. Biol.* **29**: 1342–1348.
- Buzello, M., J. Tornig, J. Faulhaber, H. Ehmke, E. Ritz, and K. Amann. 2003. The apolipoprotein E knockout mouse: a model documenting accelerated atherogenesis in uremia. *J. Am. Soc. Nephrol.* **14**: 311–316.
- Hu, W., P. Polinsky, E. Sadoun, M. E. Rosenfeld, and S. M. Schwartz. 2005. Atherosclerotic lesions in the common coronary arteries of ApoE knockout mice. *Cardiovasc. Pathol.* **14**: 120–125.
- Rattazzi, M., B. J. Bennett, F. Bea, E. A. Kirk, J. L. Ricks, M. Speer, S. M. Schwartz, C. M. Giachelli, and M. E. Rosenfeld. 2005. Calcification of advanced atherosclerotic lesions in the innominate arteries of ApoE-deficient mice: potential role of chondrocyte-like cells. *Arterioscler. Thromb. Vasc. Biol.* **25**: 1420–1425.
- Maffia, P., B. H. Zinselmeyer, A. Ialenti, S. Kennedy, A. H. Baker, I. B. McInnes, J. M. Brewer, and P. Garside. 2007. Images in cardiovascular medicine. Multiphoton microscopy for 3-dimensional imaging of lymphocyte recruitment into apolipoprotein-E-deficient mouse carotid artery. *Circulation* **115**: e326–e328.
- Yu, W., J. C. Braz, A. M. Dutton, P. Prusakov, and M. Rekhter. 2007. In vivo imaging of atherosclerotic plaques in apolipoprotein E deficient mice using nonlinear microscopy. *J. Biomed. Opt.* **12**: 054008.
- Stary, H. C., D. H. Blankenhorn, A. B. Chandler, S. Glagov, W. Insull Jr., M. Richardson, M. E. Rosenfeld, S. A. Schaffer, C. J. Schwartz, W. D. Wagner, et al. 1992. A definition of the intima of human arteries and of its atherosclerosis-prone regions. A report from the Committee on Vascular Lesions of the Council on Arteriosclerosis, American Heart Association. *Arterioscler. Thromb.* **12**: 120–134.
- Stary, H. C., A. B. Chandler, A. B. Chandler, S. Glagov, W. Insull Jr., M. Richardson, M. E. Rosenfeld, S. A. Schaffer, C. J. Schwartz, W. D. Wagner, et al. 1994. A definition of initial, fatty streak, and intermediate lesions of atherosclerosis. A report from the Committee on Vascular Lesions of the Council on Arteriosclerosis, American Heart Association. *Arterioscler. Thromb.* **14**: 840–856.
- Stary, H. C., A. B. Chandler, R. E. Dinsmore, V. Fuster, S. Glagov, W. Insull Jr., M. E. Rosenfeld, C. J. Schwartz, W. D. Wagner, and R. W. Wissler. 1995. A definition of advanced types of atherosclerotic lesions and a histological classification of atherosclerosis. A report from the Committee on Vascular Lesions of the Council on

- Arteriosclerosis, American Heart Association. *Arterioscler. Thromb. Vasc. Biol.* **15**: 1512–1531.
37. Fukumoto, S., and T. Fujimoto. 2002. Deformation of lipid droplets in fixed samples. *Histochem. Cell Biol.* **118**: 423–428.
38. Balu, M., G. Liu, Z. Chen, B. J. Tromberg, and E. O. Potma. 2010. Fiber delivered probe for efficient CARS imaging of tissues. *Opt. Express.* **18**: 2380–2388.
39. Shah, P. K., E. Falk, J. J. Badimon, A. Fernandez-Ortiz, A. Mailhac, G. Villareal-Levy, J. T. Fallon, J. Regnstrom, and V. Fuster. 1995. Human monocyte-derived macrophages induce collagen breakdown in fibrous caps of atherosclerotic plaques. Potential role of matrix-degrading metalloproteinases and implications for plaque rupture. *Circulation.* **92**: 1565–1569.
40. Aikawa, M., E. Rabkin, Y. Okada, S. J. Voglic, S. K. Clinton, C. E. Brinckerhoff, G. K. Sukhova, and P. Libby. 1998. Lipid lowering by diet reduces matrix metalloproteinase activity and increases collagen content of rabbit atheroma: a potential mechanism of lesion stabilization. *Circulation.* **97**: 2433–2444.
41. Aikawa, M., S. J. Voglic, S. Sugiyama, E. Rabkin, M. B. Taubman, J. T. Fallon, and P. Libby. 1999. Dietary lipid lowering reduces tissue factor expression in rabbit atheroma. *Circulation.* **100**: 1215–1222.
42. Massy, Z. A., O. Ivanovski, T. Nguyen-Khoa, J. Angulo, D. Szumilak, N. Mothu, O. Phan, M. Daudon, B. Lacour, T. B. Drueke, et al. 2005. Uremia accelerates both atherosclerosis and arterial calcification in apolipoprotein E knockout mice. *J. Am. Soc. Nephrol.* **16**: 109–116.
43. Aikawa, E., M. Aikawa, P. Libby, J. L. Figueiredo, G. Rusanescu, Y. Iwamoto, D. Fukuda, R. H. Kohler, G. P. Shi, F. A. Jaffer, et al. 2009. Arterial and aortic valve calcification abolished by elastolytic cathepsin S deficiency in chronic renal disease. *Circulation.* **119**: 1785–1794.